Mineralogical Magazine, October 2015, Vol. 79(5), pp. 1039–1059

Hydrothermal alteration of chevkinite-group minerals. Part 2. Metasomatite from the Keivy massif, Kola Peninsula, Russia

R. Macdonald[1,2,*], B. Bagiński[1], P. M. Kartashov[3], D. Zozulya[4] and P. Dzierżanowski[1]

[1] Institute of Geochemistry, Mineralogy and Petrology, University of Warsaw, al. Żwirki i Wigury 93, 02–089 Warsaw, Poland
[2] Environment Centre, Lancaster University, Lancaster LA1 4YQ, UK
[3] Institute of Ore Deposits, Russian Academy of Sciences, Moscow 119107, Russia
[4] Geological Institute, Kola Science Centre, Russian Academy of Sciences, Apatity, Russia

[*Received 20 January 2014; Accepted 14 January 2015; Associate Editor: K. Pfaff*]

ABSTRACT

Chevkinite-(Ce) in a mineralized quartz-epidote metasomatite from the Keivy massif, Kola Peninsula, Russia, underwent at least two stages of low-temperature alteration. In the first, it interacted with hydrothermal fluids, with loss of Ca, Fe, *LREE* and Si and strong enrichment in Ti. The altered chevkinite was then rimmed and partially replaced by a zone of ferriallanite-(Ce) and davidite-(La), in turn rimmed by a zone of allanite-(Ce) richer in the epidote component. The allanite zone was in turn partially replaced by rutile-titanite-quartz assemblages, the formation of titanite postdating that of rutile. Aeschynite-(Y), aeschynite-(Ce) and *REE*-carbonates are accessory phases in all zones. The hydrothermal fluids were alkaline, with significant proportions of CO_2 and F. At various alteration stages, the Ca, Si ± Al activities in the fluid were high. Formation of the aeschynite is discussed in relation to its stability in broadly similar parageneses; it was a primary phase in the unaltered chevkinite zone whereas in other zones it formed from Nb, Ti, *REE* and Th released from the major phases.

Keywords: chevkinite group, hydrothermal fluids, epidote supergroup, davidite, aeschynite.

Introduction

In common with studies of other *REE*- and actinide-bearing accessory minerals, it is important to understand the nature of the mobility of the rare-earth elements (*REE*, including Y), actinides (Th, U), and high-field strength elements (HFSE, e.g. Zr, Nb and Ta) during the fluid-influenced, post-magmatic stages of alteration of the chevkinite group of minerals (CGM) because the nature of the fluid-mineral chemical exchanges helps determine the availability of these elements to hydrothermal fluids and thus the mineralizing potential of the fluids (Wood and Williams-Jones, 1994; Harlov *et al*., 2011). The value of U/Pb and Th/Pb geochronological studies can also be constrained by late-stage remobilization of Th and U from accessory minerals. The compositional variations, internal zoning and alteration patterns also provide significant information on the post-magmatic history of the host rocks (Uher *et al*., 2009).

In our studies of the low-temperature alteration of the CGM, we have divided alteration schemes into two types: (1) those which started with compositional modification of the CGM and the production of a zone of 'altered chevkinite'; and (2) those where formation of this zone was followed by the formation of a new mineral assemblage. In a companion paper, Bagiński *et al*. (2015) described examples of type (1) alteration. Here we describe an example of type (2), where the CGM was initially

* E-mail: r.macdonald@lancaster.ac.uk
DOI: 10.1180/minmag.2015.079.5.02

altered by interaction with hydrothermal fluids, followed by crystallization of assemblages dominated by epidote-supergroup minerals. Hydrothermal alteration of chevkinite to allanite has been previously described by Jiang (2006); Vlach and Gualda (2007); Savel'eva and Karamanov, 2008; Hirtopanu *et al*. (2013) and Papoutsa and Pe-Piper (2013) but we believe that this report is the first record of an unusual alteration assemblage containing, in addition to epidote-supergroup minerals, davidite-(La), aeschynite-(Y), aeschynite-(Ce), niobian titanite, rutile and *REE*-carbonates.

Geological setting

The El'ozero rare-metal deposit is confined to a linear tectonic zone at the contact between the Keivy terrane and Central Kola composite terrane in the NE Fennoscandian shield (Zozulya and Eby, 2010). The zone strikes in a northwest-southeast direction for ~12 km and has an outcrop width varying from 200 to 1500 m (Fig. 1). A few hundred peralkaline A-type granite and aplite veins are confined to this zone and are concordant with the faults. The veins are from 50 to 500 m long and 3 to 50 m wide. Their age is 2.65–2.67 Ga. The granites

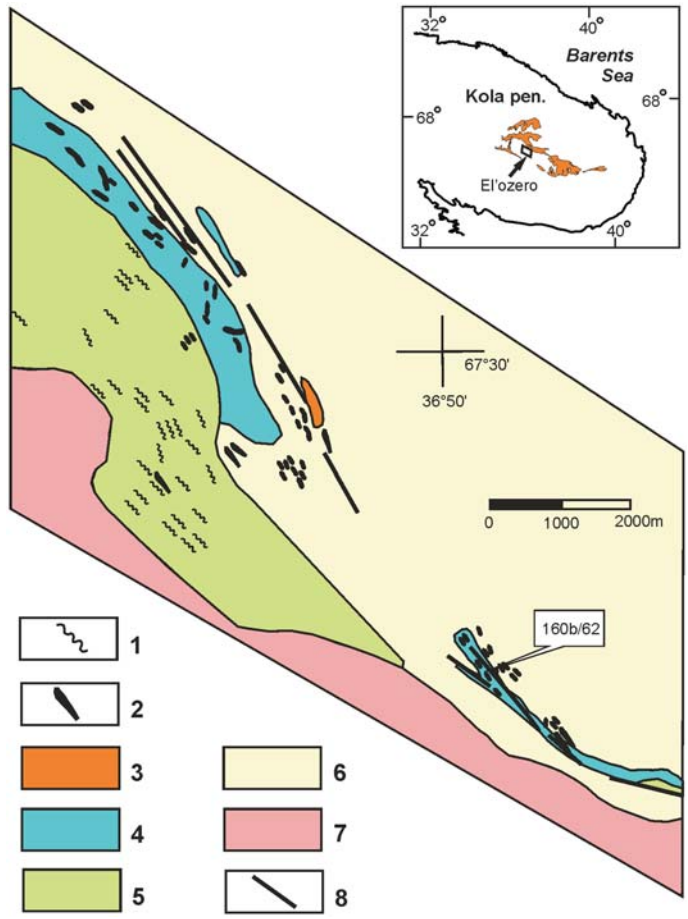

FIG. 1. Geological sketch map of the El'ozero rare-metal deposit and the location of sample 160b/62. It occurs at the contact of basic country rocks and a granite vein which is too small to show at the scale of the figure. Key to legend: 1, aplite veins; 2, mineralized granite veins; 3, aegirine-arfvedsonite granite; 4, amphibolite and basic metasomatites; 5, gabbro-anorthosite; 6, amphibole-biotite gneiss of the Keivy Terrane; 7, granite gneiss of the tonalite - tronjhemite - granodiorite basement (Central Kola Composite Terrane); 8, main faults. The inset shows the location of the Keivy peralkaline granite complex and El'ozero deposit in the Kola Peninsula.

https://doi.org/10.1180/minmag.2015.079.5.02 Published online by Cambridge University Press

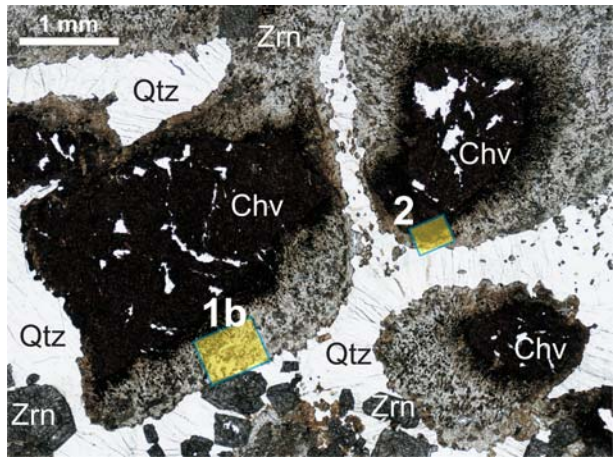

FIG. 2. Colour photomicrograph of chevkinite-(Ce) crystals in 160b/62, showing the location of areas 1b and 2. Chv, chevkinite; Qtz, quartz; Zrn, zircon.

intruded and metasomatically altered a range of rocks in the Neoarchaean Keivy gneiss complex and Keivy gabbro-anorthosite, which have ages of 2.66–2.68 Ga (Zozulya *et al*., 2001, 2005).

The Keivy peralkaline granite complex, comprising several sheet-like massifs with a total exposure of ~2500 km^2, is the only known Archaean fertile A-type granite in the world. The numerous associated Zr-Y-*REE*-Nb ore occurrences and deposits are associated with different lithologies, such as mineralized granites, quartzolites, various metasomatic rocks and pegmatites, and were formed by different genetic processes (Zozulya and Eby, 2010).

Sample 160b/62 is a metasomatite from the contact zone between a peralkaline granite vein and basic country rocks (gabbro-anorthosite, amphibolite) at the El'ozero occurrence, West Keivy massif. The vein is too small to show on the scale of Fig. 1. The sample is from an irregularly-shaped, veined body up to 1 m long of heavily mineralized Ca-Na-amphibole-lepidomelane-aegirine-quartz-feldspar-epidote metasomatite. The associated rare-metal mineralization includes, in addition to chevkinite-(Ce), zircon, thorite, allanite-ferriallanite-(Ce), fergusonite-(Y), gadolinite-group minerals, pyrochlore, fluorite, cassiterite, crichtonite-group minerals, danalite and monazite-(Ce). The body is thought to have formed by fenitization and later silicification of amphibolites by granite-derived fluids.

Full details of the analytical conditions used are given in Bagiński *et al*. (2015) and will not be repeated here.

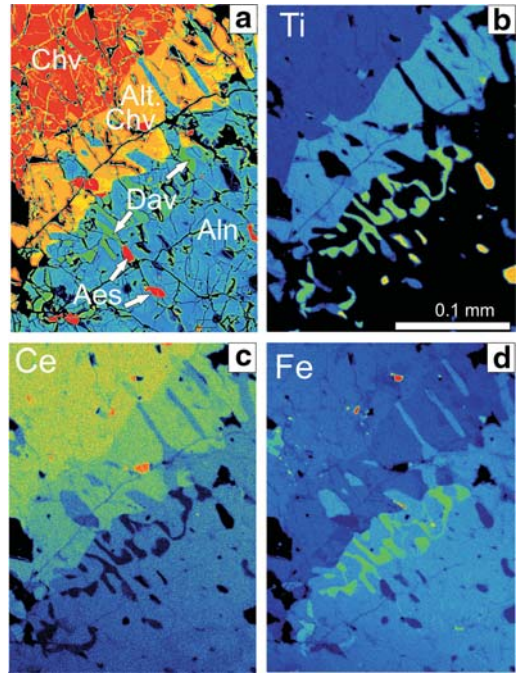

FIG. 3. (*a*) False colour BSE image of chevkinite-allanite relationships in sample 160b/62 (area 2). The orange area is unaltered chevkinite-(Ce), yellow is altered chevkinite. Blue is ferriallanite-(Ce), which also forms fingers and patches in the altered chevkinite. The green phase is davidite-(La), which becomes less abundant away from the chevkinite. Aeschynite-(Y) and aeschynite-(Ce) crystals are red. (*b–d*) Distribution of Ti, Ce and Fe in the same area as image (*a*).

https://doi.org/10.1180/minmag.2015.079.5.02 Published online by Cambridge University Press

Textural relationships

Deep-red crystals of chevkinite-(Ce) are shown in Fig. 2, up to 3 mm across, with grey mottled rims of alteration products up to 1.5 mm thick, set in a matrix of quartz which also appears to penetrate the chevkinite-(Ce) as veinlets. Associated with the quartz are abundant euhedral crystals of zircon. Areas marked as 1b and 2 show the transition from chevkinite-(Ce) to its alteration rim and were previously featured in Bagiński *et al*. (2015). Areas 1b and 2 have a similar alteration pattern and are subsequently treated together here as crystals 1b/2.

Area 2 is shown as a false-colour backscattered electron (BSE) image in Fig. 3*a*. The orange zone is unaltered chevkinite-(Ce). The yellow material mantling the chevkinite-(Ce), and apparently forming along cracks within it, is altered chevkinite. The altered phase is in turn rimmed by a zone which is mainly a mixture of ferriallanite-(Ce) (blue) and davidite-(La) (green). The ferriallanite-(Ce) also forms fingers and patches which penetrate the altered chevkinite and, more rarely, the unaltered chevkinite-(Ce). The small (≤20 μm) bright red phases are aeschynite-(Ce) and aeschynite-(Y). The distributions of Fe, Ti and Ce over the

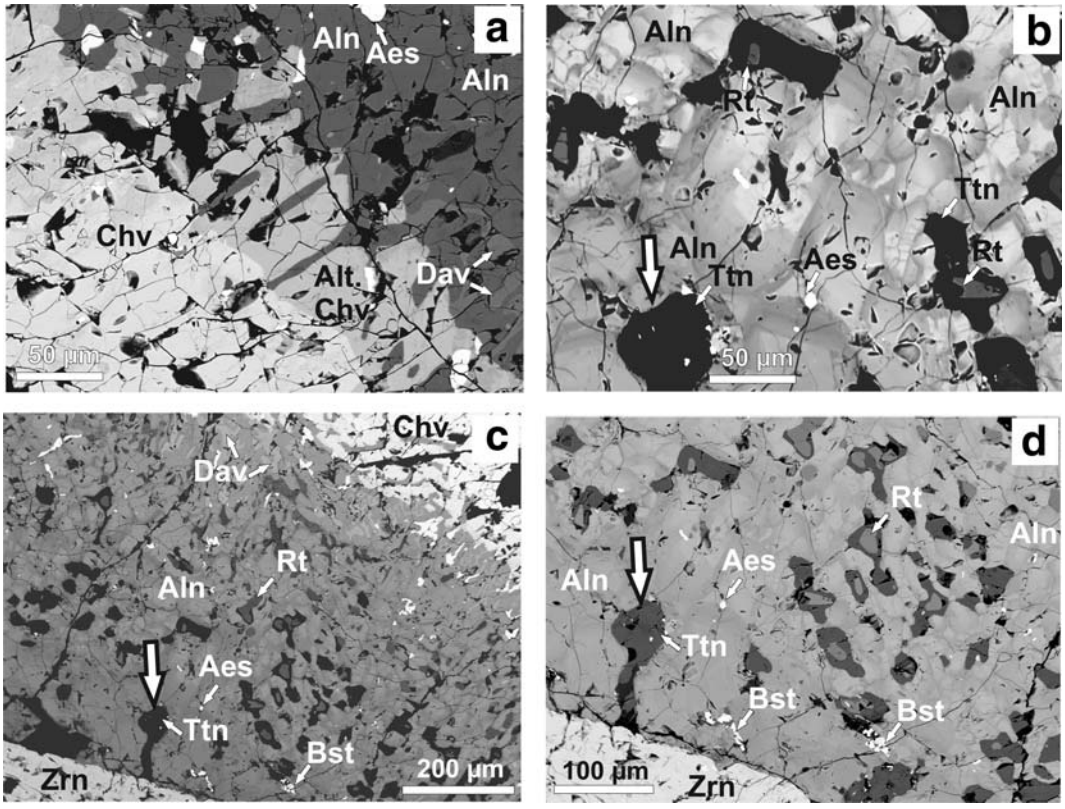

FIG. 4. BSE images of various components of the altered rim, sample 160b/62. (*a*) The main mottled area comprises ferriallanite-(Ce) (slightly darker; Aln) and davidite-(La) (lighter; Dav). Aeschynite-(Y) grains (Aes) are bright. The davidite grains are more rounded than those nearer the contact with the altered chevkinite (Chv). (*b*) In detail, the allanite-(Ce) (Aln) comprises darker and lighter components, varying in Ca/*REE* proportions. The dark areas with medium grey 'cores' are titanite (Ttn) mantling rutile (Rt) and the bright crystals are aeschynite-(Y). (*c*) Rutile forms medium-grey, rounded to elongate grains surrounded by dark titanite. (*d*) More general view of the increase in the proportions of titanite and rutile further from the contact with altered chevkinite.The 'tadpole'-shaped area in the bottom-left contains titanite and quartz, partially replaced by chlorite. The small bright grains are aeschynite-(Y) and hydroxylbastnäsite-(Ce) (Bst). The zircon (Zrn) at the bottom of the image is taken to be a primary phase.

https://doi.org/10.1180/minmag.2015.079.5.02 Published online by Cambridge University Press

same area highlight in particular the zone of altered chevkinite (Figs 3*b–d*).

On standard BSE images, the unaltered chevkinite-(Ce) is slightly brighter (higher *Z*) than the altered phase (Fig. 4*a*). In detail, the allanite-(Ce) consists of two components, lighter (mainly ferriallanite-(Ce)) and darker (allanite-(Ce)), especially further from the altered chevkinite zone (Fig. 4*b*). The darker component appears to be later than the lighter. The davidite-(La) is slightly brighter on the BSE images and is intimately intergrown with the ferriallanite-(Ce). Nearest the contact with the altered chevkinite, the davidite-(La) forms elongated stringers, sometimes growing at right angles to the contact (Figs 3*a*, 4*a*). Further from the contact, it takes a more rounded form (Fig. 4*c*), becomes much less abundant and eventually disappears. Rutile forms isolated dark grey patches near the contact with the altered chevkinite; at ~300 μm from the contact, the rutile occurs in a concentration of irregularly shaped patches as cores surrounded by titanite, very dark on the BSE images (Fig. 4*d*). The tadpole-shaped bleb contains titanite and quartz partially surrounded by chlorite. Rare hydroxylbastnäsite-(Ce), sometimes associated with quartz, and britholite-(Ce) grains occur near the contact with a zircon crystal which is assumed to have been primary.

Mineral compositions

Chevkinite-(Ce) and altered chevkinite

The general formula for chevkinite is $A_4BC_2D_2(Si_2O_7)_2O_8$, where the dominant cations in each site are: A = Ca, *REE*; B = Fe^{2+}; C = Fe^{2+}, Fe^{3+}, Ti, Zr; D = Ti. Formulae in this paper were calculated on the basis of 22 oxygens and with all Fe as Fe^{2+}. The unaltered phase is chevkinite-(Ce), with high *REE* + Y contents (average 3.76 atoms per formula unit (a.p.f.u.)) and low Ca (0.32 a.p.f.u.), and with notably low Zr (0.002 a.p.f.u.), Th (0.027 a.p.f.u.) and Nb (0.054 a.p.f.u.) contents (Macdonald *et al*., 2012). The *C* site is dominated by Fe^{2+} (0.992 a.p.f.u.). Its classification as chevkinite is explained in Bagiński *et al*. (2015). The sample is not compositionally unusual compared to published compositions of chevkinite-(Ce) (see compilations in Macdonald and Belkin, 2002; Vlach and Gualda, 2007; Carlier and Lorand, 2008; Belkin *et al*., 2009; Macdonald *et al*., 2009, 2012, 2013). Chondrite-normalized *REE* patterns show strong *LREE* enrichment (Fig. 5).

Progressive alteration of the chevkinite-(Ce), described in detail by Bagiński *et al*. (2015), is represented by the analyses of unaltered, partly altered and strongly altered varieties in Table 1. Loss of Ca and *LREE* from the strongly altered

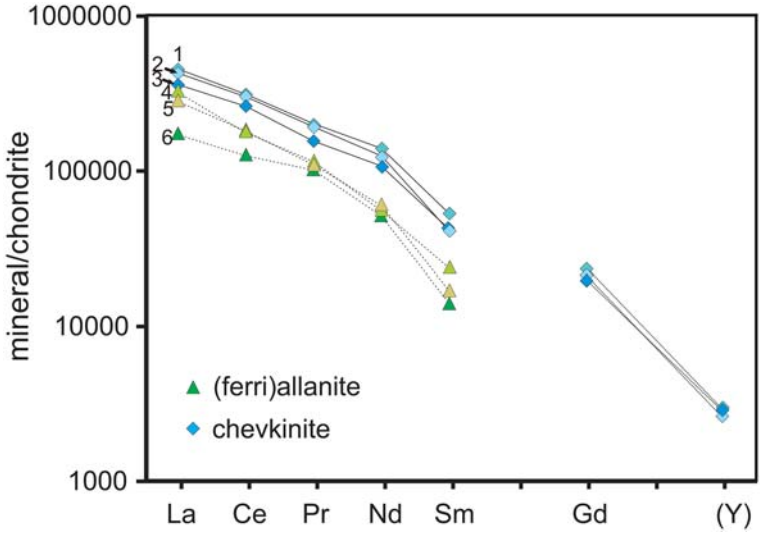

FIG. 5. Chondrite-normalized *REE* patterns for chevkinite and allanite. Y proxies for Ho. Chevkinite: 1, unaltered; 2, partly altered; 3, strongly altered (averages, Table 1). Ferriallanite/allanite: 4, finger in altered chevkinite; 5, in main ferriallanite-(Ce) zone, with davidite-(La); 6, dark patch distant from altered chevkinite. Analyses used; Supplementary Table 2*a*, numbers 3, 9, 14. Normalizing factors from Sun and McDonough (1989).

https://doi.org/10.1180/minmag.2015.079.5.02 Published online by Cambridge University Press

TABLE 1. EMP analytical results for alteration phases in chevkinite-(Ce), sample 160b/62.

	Unaltered			Partly altered			Strongly altered		
n	5			4			11		
	average	min	max	average	min	max	average	min	max
wt.%									
P_2O_5	0.02	b.d.	0.02	0.02	0.01	0.02	0.03	b.d.	0.06
Nb_2O_5	0.61	0.43	0.83	0.67	0.60	0.73	0.94	0.52	1.47
Ta_2O_5	0.12	b.d.	0.15	0.13	0.10	0.17	0.13	b.d.	0.17
SiO_2	18.58	18.34	18.70	18.32	17.40	19.05	14.86	14.56	16.68
TiO_2	16.36	15.54	17.04	17.43	16.31	18.98	31.49	30.04	33.35
ThO_2	0.89	0.49	1.12	0.94	0.79	1.14	1.14	0.74	1.84
Al_2O_3	0.42	0.16	0.66	0.38	0.33	0.46	0.10	0.04	0.39
Y_2O_3	0.50	0.42	0.67	0.58	0.55	0.60	0.54	0.35	0.78
La_2O_3	12.61	11.90	13.21	11.82	11.02	12.95	9.97	8.62	10.56
Ce_2O_3	22.52	21.74	23.23	21.71	21.34	22.38	18.50	17.40	19.32
Pr_2O_3	2.17	1.99	2.49	2.10	1.97	2.22	1.73	1.37	2.02
Nd_2O_3	7.35	7.00	7.80	6.59	6.15	7.40	5.84	5.24	7.28
Sm_2O_3	0.92	0.78	1.10	0.72	0.63	0.84	0.76	0.53	1.05
Gd_2O_3	0.48	0.33	0.65	0.57	0.30	0.72	0.44	0.27	0.63
MgO	0.16	0.15	0.19	0.08	0.05	0.10	0.06	0.04	0.08
CaO	1.45	1.29	1.75	2.58	1.51	3.36	1.08	0.48	2.96
MnO	0.26	0.24	0.29	0.41	0.19	0.61	0.23	0.18	0.27
FeO*	10.87	10.54	11.29	7.73	5.42	10.02	8.53	3.05	10.03
SrO	0.05	b.d.	0.05	0.03	0.02	0.05	0.04	b.d.	0.04
BaO	0.24	0.18	0.30	0.13	0.05	0.18	0.19	b.d.	0.26
Na_2O	b.d.	b.d.	b.d.	0.06	0.02	0.10	0.12	b.d.	0.12
Total	96.40	94.17	97.61	93.07	91.45	93.98	96.49	94.44	97.96
Formulae based on 22 oxygen									
Ca	0.342	0.302	0.421	0.613	0.359	0.817	0.235	0.104	0.643
Sr	0.003	0.000	0.006	0.004	0.003	0.007	0.001	0.000	0.005
Ba	0.008	0.000	0.026	0.008	0.000	0.016	0.007	0.000	0.021
Na	0.000	0.000	0.000	0.013	0.000	0.043	0.004	0.000	0.047
La	1.019	0.959	1.058	0.969	0.905	1.084	0.746	0.645	0.792

Table 1 (*contd.*)

Ce	1.807	1.739	1.851	1.767	1.698	1.86	1.374	1.293	1.438
Pr	0.174	0.158	0.198	0.17	0.16	0.176	0.128	0.101	0.149
Nd	0.575	0.542	0.609	0.523	0.477	0.588	0.423	0.376	0.527
Sm	0.070	0.059	0.082	0.055	0.048	0.063	0.053	0.037	0.073
Gd	0.035	0.024	0.047	0.042	0.023	0.053	0.030	0.018	0.043
Y	0.058	0.049	0.078	0.069	0.066	0.07	0.059	0.038	0.084
Th	0.044	0.024	0.056	0.047	0.041	0.058	0.053	0.034	0.085
Sum *A*	4.134	4.100	4.236	4.279	4.052	4.659	3.112	2.994	3.535
Fe^{2+}	1.000	1.000	1.000	1.000	1.000	1.000	0.940	0.517	1.000
Mn	0.000	0.000	0.000	0.000	0.000	0.000	0.007	0.000	0.041
Mg	0.000	0.000	0.000	0.000	0.000	0.000	0.001	0.000	0.015
Sum *B*	1.000	1.000	1.000	1.000	1.000	1.000	0.948	0.551	1.000
Fe^{2+}	0.992	0.975	1.045	0.437	0.009	0.86	0.508	0.000	0.686
Mn	0.048	0.044	0.054	0.078	0.036	0.112	0.033	0.000	0.046
Mg	0.054	0.048	0.062	0.027	0.017	0.033	0.015	0.000	0.024
Nb	0.061	0.042	0.081	0.067	0.06	0.075	0.086	0.048	0.134
Ta	0.006	0.000	0.009	0.008	0.006	0.01	0.006	0.000	0.009
Al	0.108	0.041	0.170	0.100	0.085	0.121	0.023	0.010	0.093
Ti	0.695	0.626	0.788	0.911	0.785	1.177	2.806	2.572	3.088
Sum *C*	1.962	1.839	2.023	1.631	1.436	1.925	3.478	2.738	3.674
Ti (=*D*)	2.000	2.000	2.000	2.000	2.000	2.000	2.000	2.000	2.000
Si	4.070	4.036	4.121	4.068	3.950	4.140	3.016	2.955	3.375
P	0.001	0.000	0.004	0.002	0.000	0.004	0.004	0.000	0.010
Sum *T*	4.071	4.038	4.121	4.07	3.954	4.144	3.020	2.960	3.380
Σ cations	13.17	13.14	13.20	12.98	12.70	13.14	12.56	12.28	12.63

From data in Macdonald *et al.* (2012) and this work.
FeO*, all Fe as Fe^{2+}. *n*, number of analyses used in averages. b.d., below detection.

TABLE 2. Representative EMP analytical data for ferriallanite and allanite in 160b/62.

Sample no.	1	2	3	4	5	6	7	8
wt.%								
SiO_2	29.75	29.41	30.31	29.19	30.39	31.58	31.75	30.25
TiO_2	1.18	2.42	1.60	1.77	0.86	0.42	0.23	0.41
ThO_2	0.15	b.d.	0.21	0.20	0.19	0.48	0.44	0.21
Al_2O_3	11.48	12.75	13.55	9.62	14.45	16.46	17.45	15.13
Y_2O_3	0.14	0.08	0.09	0.03	0.10	0.61	0.53	b.d.
La_2O_3	6.26	9.23	8.56	8.75	8.44	5.34	4.79	8.73
Ce_2O_3	12.31	13.18	12.99	13.73	13.04	10.19	9.13	13.06
Pr_2O_3	1.44	1.29	1.23	1.31	1.06	0.84	1.16	0.90
Nd_2O_3	5.05	2.92	2.94	2.90	3.44	3.84	3.17	3.06
Sm_2O_3	0.58	0.44	0.36	0.34	0.30	0.45	0.31	0.18
Gd_2O_3	0.34	b.d.	b.d.	b.d.	b.d.	0.33	0.38	b.d.
MgO	0.47	0.48	0.42	0.56	0.43	0.32	0.29	0.44
CaO	8.95	8.76	9.21	9.20	9.14	11.18	12.53	9.55
MnO	0.14	0.24	0.11	0.20	0.35	0.13	0.26	0.09
FeO*	16.48	15.27	14.97	18.64	14.34	13.21	12.54	13.89
Na_2O	b.d.	0.03	0.04	b.d.	0.06	0.12	b.d.	b.d.
Total	94.72	96.50	96.72	96.44	96.75	95.50	94.96	95.90
Formulae based on 12.5 oxygens								
Ca	0.999	0.954	0.989	1.032	0.979	1.163	1.289	1.025
Na	0.000	0.006	0.008	0.000	0.012	0.023	0.000	0.000
La	0.241	0.346	0.316	0.338	0.311	0.191	0.170	0.323
Ce	0.470	0.490	0.477	0.526	0.477	0.362	0.321	0.479
Pr	0.055	0.048	0.045	0.050	0.039	0.030	0.041	0.033
Nd	0.188	0.106	0.105	0.108	0.123	0.133	0.109	0.109
Sm	0.021	0.015	0.012	0.012	0.010	0.015	0.010	0.006
Gd	0.012	0.000	0.000	0.000	0.000	0.011	0.000	0.000
Y	0.008	0.004	0.005	0.002	0.005	0.032	0.027	0.000
Th	0.004	0.000	0.005	0.005	0.004	0.011	0.010	0.005
Sum *A*	1.996	1.970	1.962	2.073	1.960	1.969	1.975	1.980
Fe^{2+}	1.436	1.298	1.255	1.631	1.198	1.072	1.007	1.164
Mn	0.012	0.021	0.009	0.018	0.030	0.011	0.021	0.008
Mg	0.073	0.073	0.063	0.087	0.064	0.046	0.041	0.066
Al	1.410	1.527	1.601	1.187	1.702	1.883	1.974	1.787
Ti	0.092	0.185	0.121	0.139	0.065	0.031	0.017	0.031
Sum *M*	3.024	3.103	3.055	3.062	3.063	3.043	3.060	3.055
Si	3.100	2.988	3.038	3.055	3.037	3.065	3.047	3.031
Σ cations	8.12	8.06	8.05	8.19	8.06	8.08	8.08	8.07

1, in the chevkinite zone; 2, 3, fingers in altered chevkinite zone; 4, dark patch in altered chevkinite zone; 5,6, intergrown with davidite-(La); 7, 8, intergrown with titanite; b.d., below detection. FeO*, all Fe as Fe^{2+}.

varieties led to a deficiency in the *A* site (minimum 2.99 a.p.f.u.), loss of Si (minimum sum of *T* cations = 2.96 a.p.f.u.) and enrichment in Ti (maximum total Ti = 5.09 a.p.f.u.). Thus, the composition of the altered material cannot be simply represented by the standard chevkinite formula. Loss of *LREE* did not result in significant fractionation of the *REE* (Fig. 5). We stress that no information is yet available on the nature and structure of the so-called 'altered chevkinite', which may or may not be a member of the chevkinite group.

Epidote supergroup

Epidote-supergroup formulae have been calculated on the basis of 12.5 oxygens per formula unit (Table 2 and Supplementary Table 2*a* which has

https://doi.org/10.1180/minmag.2015.079.5.02 Published online by Cambridge University Press

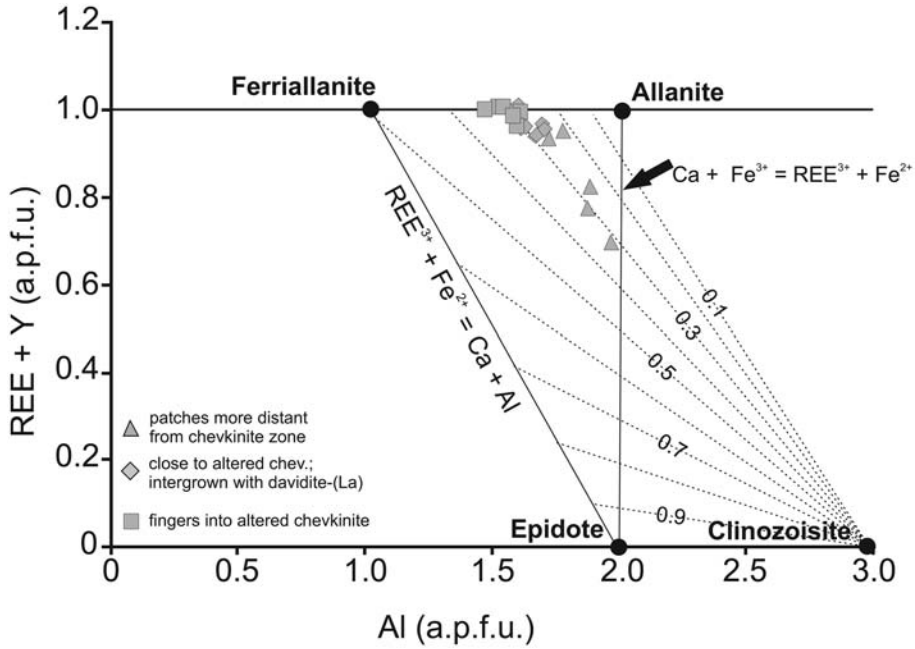

FIG. 6. Epidote-supergroup minerals in 160b/62 plotted in the (*REE* + Th + Mn + Sr) *vs*. Al diagram of Petrik *et al*. (1995), contoured with isolines of the ratio $Fe^{3+}/(Fe^{3+} + Fe^{2+})$. The plot indicates the substitutions allanite – epidote (Ca + Fe^{3+} = *REE* + Fe^{2+}); ferriallanite – epidote (Ca + Al = *REE* + Fe^{2+}); and ferriallanite – allanite (Fe^{3+} = Al).

been deposited with the Principal Editor of *Mineralogical Magazine* and is available from www.minersoc.org/pages/e_journals/dep_mat_mm.html). Compositions are plotted in the (*REE* + Y + Sr + Th) *vs*. Al diagram of Petrik *et al*. (1995) (Fig. 6). Compositional variations are partly related to distance from the altered chevkinite zone. The phases occurring as fingers and patches in that zone have a slightly higher ferriallanite component than those intergrown with davidite-(La). The darker phase in the zone furthest from the altered chevkinite plots towards the epidote-allanite join. All the phases have Ce as the dominant *REE* and are thus ferriallanite-(Ce) and allanite-(Ce). The $Fe^{3+}/(Fe^{3+} + Fe^{2+})$ ratios, calculated from stoichiometry, for the transition ferriallanite-(Ce) to allanite-(Ce) show an overall increase from 0.14 to 0.30. Titanium values increase with decreasing Al content, up to 0.19 a.p.f.u.

Thus, during successive phases of formation, and assuming that the phase in, and immediately rimming, the altered chevkinite zone formed first, the allanite had progressively higher Ca and Al and lower *REE*, Fe and Ti (c.f. Petrik *et al*., 1995). Increasing epidote component was accompanied by a modest decrease in the $[La/Nd]_{CN}$ ratio, from 6 to ~3 (Fig. 5), and a strong decrease in the $[La/Y]_{CN}$ ratio, from ~1500 to 65. Compositionally similar, post-magmatic allanite-(Ce) forming rims around chevkinite-(Ce) has been described in the Shuiquangou syenitic intrusion, northern China, by Jiang (2006) and in the Farinha Seca syenitic pluton, Graciosa Province, by Vlach and Gualda (2007).

Davidite-(La)

Davidite is a member of the crichtonite group of minerals. Various versions of the formula have been suggested (Gatehouse *et al*., 1979; Haggerty *et al*., 1983; Olerud, 1988); here we adopt the format presented by Back and Mandarino (2008), distinguishing three species: davidite-(Ce) – (Ce, La)(Y, U,Fe^{2+})(Ti,Fe^{3+})$_{20}$(O,OH)$_{38}$; davidite-(La) – (La, Ce)(Y,U,Fe^{2+})(Ti,Fe^{3+})$_{20}$(O,OH)$_{38}$; and davidite-(Y) – (Y,U)(Ti,Fe^{3+})$_{21}$O$_{38}$. Compositions of davidite in 160b/62 are given in Table 3, along with formulae calculated on the basis of 22 cations and with all Fe as Fe^{2+}. Calcium, Sr, Ba and Na have been allocated to the same site as Y, U and Fe^{2+}. They are minor components; e.g. the sum of (Sr + Ba + Na), is <0.04 a.p.f.u. The heavy rare-earth

https://doi.org/10.1180/minmag.2015.079.5.02 Published online by Cambridge University Press

TABLE 3. EMP analytical results for davidite-(La) in 160b/62.

	Intergrown with (ferri)allanite			Blebs and stringers in (ferri)allanite zone				
Analyses no.	1	2	3	4	5	6	7	8
wt.%								
P_2O_5	b.d.	0.04	b.d.	b.d.	0.04	b.d.	0.06	b.d.
Nb_2O_5	0.67	1.07	1.18	0.94	0.94	1.29	1.39	1.06
Ta_2O_5	b.d.	0.05	0.08	b.d.	b.d.	0.08	b.d.	b.d.
SiO_2	0.02	b.d.	0.04	0.01	b.d.	0.26	0.24	0.20
TiO_2	56.38	55.29	54.96	55.59	55.52	53.51	52.60	55.06
ZrO_2	0.24	0.18	0.11	0.18	0.18	b.d.	b.d.	0.17
ThO_2	0.49	0.71	0.48	0.29	0.34	0.25	0.18	0.39
UO_2	0.13	b.d.	0.47	0.29	0.29	0.22	0.25	0.26
Al_2O_3	0.17	0.20	0.21	0.20	0.15	0.19	0.16	0.19
Y_2O_3	3.27	3.30	3.19	3.34	3.27	3.34	3.45	3.31
La_2O_3	4.12	4.19	3.69	4.29	4.47	4.44	4.38	4.22
Ce_2O_3	3.48	3.19	2.85	3.33	3.40	3.19	3.06	3.12
Pr_2O_3	0.31	0.09	0.20	b.d.	b.d.	b.d.	b.d.	0.20
Nd_2O_3	0.46	0.53	0.57	0.46	0.32	0.70	0.42	0.40
Gd_2O_3	0.42	0.42	0.46	0.46	0.54	0.46	0.66	0.56
Dy_2O_3	b.d.	0.37	0.54	b.d.	b.d.	b.d.	b.d.	0.55
Er_2O_3				0.34	0.35	0.48	0.49	0.55
Yb_2O_3	0.75	0.67	0.89	0.58	0.68	0.78	0.84	0.82
MgO	0.04	0.04	0.02	0.04	0.03	0.07	0.04	0.07
CaO	0.22	0.24	0.32	0.37	0.38	0.32	0.35	0.33
MnO	0.35	0.28	0.32	0.3	0.31	0.37	0.29	0.35
FeO*	19.84	22.67	21.62	20.94	20.63	21.98	21.60	21.11
BaO	0.14	0.25	b.d.	b.d.	b.d.	b.d.	b.d.	b.d.
Total	91.50	93.78	92.20	91.95	91.84	91.93	90.46	92.92

(continued)

Table 3 (*contd.*)

Formulae based on 22 cations								
La	0.508	0.505	0.452	0.526	0.551	0.546	0.548	0.516
Ce	0.426	0.381	0.347	0.406	0.416	0.390	0.380	0.378
Pr	0.038	0.011	0.024	0.000	0.000	0.000	0.000	0.024
Nd	0.055	0.062	0.068	0.055	0.038	0.083	0.051	0.047
Sum *LREE*	1.027	0.959	0.891	0.987	1.005	1.019	0.979	0.966
Ca	0.079	0.084	0.114	0.132	0.136	0.114	0.127	0.117
Ba	0.018	0.032	0.000	0.000	0.000	0.000	0.000	0.000
Gd	0.047	0.045	0.051	0.051	0.060	0.051	0.074	0.062
Dy	0.000	0.039	0.058	0.000	0.000	0.000	0.000	0.059
Er	0.000	0.000	0.000	0.051	0.037	0.050	0.052	0.057
Yb	0.077	0.067	0.090	0.059	0.069	0.079	0.087	0.083
Y	0.582	0.574	0.564	0.591	0.582	0.593	0.623	0.584
Th	0.037	0.053	0.036	0.022	0.026	0.019	0.014	0.029
U	0.010	0.000	0.035	0.021	0.022	0.016	0.019	0.019
Sum	0.849	0.894	0.948	0.927	0.931	0.923	0.996	1.010
Fe^{2+}	5.551	6.192	6.010	5.825	5.766	6.132	6.127	5.848
Mn	0.099	0.077	0.090	0.085	0.088	0.105	0.083	0.098
Mg	0.020	0.019	0.010	0.020	0.015	0.035	0.020	0.035
Zr	0.039	0.029	0.018	0.029	0.029	0.000	0.000	0.027
Nb	0.101	0.158	0.177	0.141	0.142	0.195	0.213	0.159
Ta	0.000	0.004	0.007	0.000	0.000	0.007	0.000	0.000
Al	0.067	0.077	0.082	0.078	0.059	0.075	0.064	0.074
Ti	14.184	13.580	13.739	13.905	13.954	13.423	13.418	13.717
Si	0.007	0.000	0.013	0.003	0.000	0.087	0.081	0.066
P	0.000	0.011	0.000	0.000	0.011	0.000	0.017	0.000
Sum	20.068	20.148	20.148	20.087	20.064	20.058	20.025	20.025

b.d., below detection; blank, not determined.
FeO*, all Fe as Fe^{2+}.

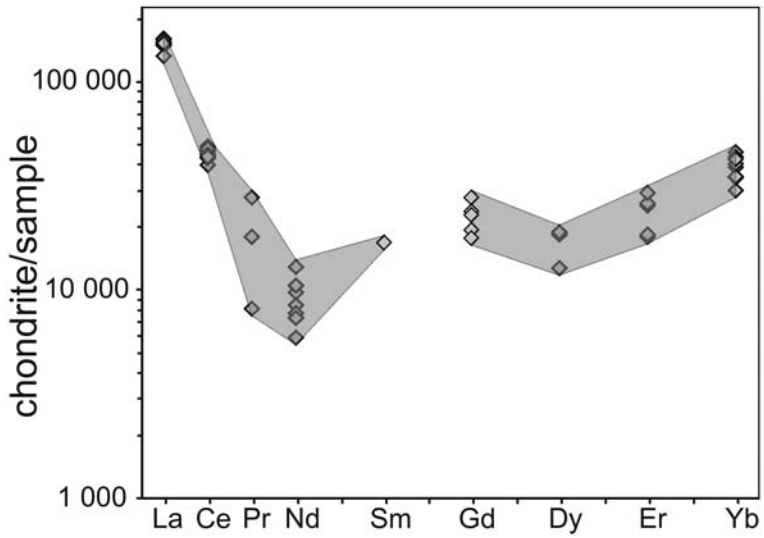

FIG. 7. Chondrite-normalized *REE* patterns for davidite-(La). Normalizing factors from Sun and McDonough (1989). Source data from Table 3.

elements (*HREE*) have also been put into that site. Chromium and V were sought but not detected. The formula can be written in simplified form as $(LREE_{0.98})(Y_{0.59}HREE_{0.18}Ca_{0.11}Th_{0.03}U_{0.02})_{0.93}(Ti_{13.74}Fe^{2+}_{5.93}Nb_{0.16}Mn_{0.09}Al_{0.07})_{19.99}(O_{34}OH_5)$, with the proportions of O and OH being calculated from charge balance. The content of La is 0.52 a.p.f.u. and of Ce 0.39 a.p.f.u., making the phase davidite-(La). Although our *REE* data are incomplete, it is clear from the chondrite-normalized patterns (Fig. 7) that the davidite-(La) shows the dip in the middle *REE* and renewed enrichment in the *HREE* previously recorded in davidite (Gatehouse *et al*., 1979; Green and Pearson, 1987; Olerud, 1988). The abundances of the minor elements, such as Zr, Nb and Th, are in line with analyses published by Gatehouse *et al*. (1979) of davidite from Arizona, Norway and South Australia.

Davidite is known from a wide range of alkaline igneous rocks, granitic pegmatites and hydrothermal deposits. It occurs intergrown with ilmenite and rutile in the type locality, Radium Hill, South Australia (Gatehouse *et al*., 1979). In contrast to the Keivy association, Chakmouradian and Mitchell (1999) reported crichtonite as reaction rims on rutile in nepheline syenite pegmatites of Pegmatite Peaks, Bearpaw Mountains, Montana. Our sample appears to be the first record of a crichtonite-group mineral replacing, along with ferriallanite-(Ce), a chevkinite-group mineral.

Rutile and titanite

Analyses of Nb-bearing rutile are presented in Table 4. Oxide totals are in the range 100.10–100.53 wt.% and the sum of cations is 1.01–1.02 a.p.f.u. The rutile has the average composition $(Ti_{0.86}Nb_{0.08}Fe^{2+}_{0.07})O_2$, with a small range of Ti values (0.85–0.88 a.p.f.u.). Niobium levels range from 0.066–0.090 a.p.f.u. (10.30–14.02 wt.% Nb_2O_5). Tantalum levels are low (<0.7 wt.% Ta_2O_5) and Nb/Ta ratios correspondingly high (34–67). Iron contents are modest (4.97–6.11 wt.% FeO*, where FeO* is all Fe as Fe^{2+}), whilst Mn levels are below detection in all but one analysis (0.06 wt.% MnO). Tin (as SnO_2) abundances are between 0.28 and 0.36 wt.%. Such levels are low; e.g. René and Škoda (2011), reported SnO_2 abundances from 0.5–5.3 wt.% in rutile from the Krásno-Horni Slavkov ore district, Czech Republic.

The ideal formula for titanite is $CaTiOSiO_4$. The titanite in 160b/62 has the average composition $(Ca_{0.93}Y_{0.06})_{0.99}(Ti_{0.74}Al_{0.26}Fe^{3+}_{0.03})Si_{1.02}O_4$ (Table 4). The Al_2O_3 content, up to 7.05 wt.% (Al 0.28 a.p.f.u.), is unusually, but not exceptionally, high. Wang *et al*. (2001), for example, reported Al_2O_3 levels of 9.3–11.7 wt.% in secondary titanite in the Laoshan granitic complex, Eastern China, and Xie *et al*. (2006) recorded up to 9.4 wt.% Al_2O_3 in titanite from the aluminous A-type Xincun granite,

https://doi.org/10.1180/minmag.2015.079.5.02 Published online by Cambridge University Press

TABLE 4. EMP analytical results for rutile and titanite in 160b/62.

	Rutile					Titanite		
Analyses No.	1	2	3	4	5	6	7	8
wt.%								
Nb_2O_5	14.02	11.62	13.79	12.54	10.30	0.26	0.24	0.20
Ta_2O_5	0.60	0.29	0.68	0.44	0.28			
SiO_2	0.04	0.04	0.01	0.07	0.24	30.11	29.65	29.81
TiO_2	79.14	82.25	79.25	80.29	82.69	28.25	29.02	29.23
SnO_2	0.35	0.28	0.35	0.36				
Fe_2O_3*						1.10	1.43	1.47
Al_2O_3	0.03	b.d.	b.d.	0.06	0.04	7.05	6.32	6.25
Y_2O_3	b.d.	b.d.	b.d.	b.d.	b.d.	3.36	3.48	3.50
MgO	b.d.	0.01	b.d.	b.d.	b.d.	0.14	0.14	0.13
CaO	0.24	0.17	0.22	0.65	0.29	25.56	25.33	25.13
MnO	b.d.	0.06	b.d.	b.d.	b.d.	0.13	0.14	0.13
FeO*	6.11	5.40	6.12	5.69	4.97			
Na_2O						0.21	0.24	0.21
F						2.20	2.03	1.65
Sum	100.53	100.12	100.42	100.10	98.81	98.37	98.02	97.71
O = F						0.93	0.85	0.69
Total	100.53	100.12	100.42	100.10	98.81	97.44	97.17	97.02
Formulae based on two oxygens							Based on three cations	
Ca	0.004	0.003	0.003	0.010	0.004	0.908	0.906	0.899
Na						0.013	0.016	0.014
Y	0.000	0.000	0.000	0.000	0.000	0.059	0.062	0.062
Fe^{2+}	0.072	0.064	0.073	0.067	0.059			
Fe^{3+}						0.027	0.036	0.037
Mn	0.000	0.001	0.000	0.000	0.000	0.003	0.004	0.004
Mg	0.000	0.000	0.000	0.000	0.000	0.007	0.007	0.006
Nb	0.090	0.074	0.089	0.080	0.066	0.004	0.004	0.003
Ta	0.002	0.001	0.003	0.002	0.001			
Al	0.000	0.000	0.000	0.001	0.001	0.275	0.249	0.246
Ti	0.844	0.871	0.846	0.855	0.881	0.704	0.728	0.734
Si	0.000	0.000	0.000	0.000	0.003	0.998	0.989	0.995
Sn	0.002	0.002	0.002	0.002				
F						0.231	0.214	0.174
Σ cations	1.02	1.01	1.02	1.02	1.02			

All rutile analyses in small (25 μm x 10 μm) cores to titanite grains. Titanite associated with chlorite in allanite zone.
FeO*, all Fe as Fe^{2+}. Fe_2O_3*, all Fe as Fe^{3+}. b.d., below detection. Blanks, not determined.

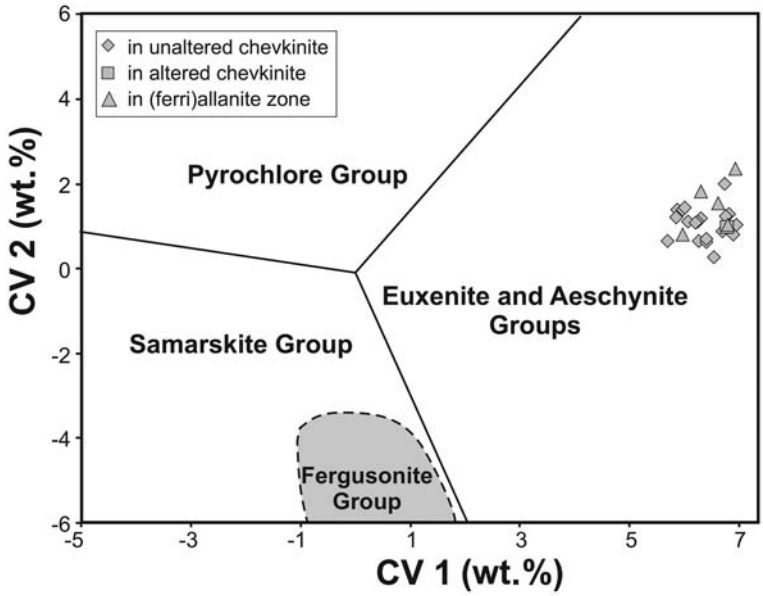

FIG. 8. Aeschynite in Keivy sample 160b/62 plotted as canonical variables CV1 and CV2 of the three-group model of Ercit (2005). Data from Supplementary Table 2*b*. CV1 = 0.245 Na + 0.106 Ca – 0.077 Fe* + 0.425 Pb + 0.220 Y + 0.280 *LREE* + 0.137 *HREE* + 0.100 U* + 0.304 Ti + 0.097 Nb + 0.109 Ta* –12.81 (oxide wt.%). CV2 = 0.102 Na – 0.113 Ca – 0.371 Fe* – 0.167 Pb – 0.395 Y – 0.280 *LREE* – 0.265 *HREE* – 0.182 U* – 0.085 T – 0.166 Nb – 0.146 Ta* + 17.29 (oxide wt.%). Fe* = Fe + Mn; U* = U + Th; Ta* = Ta + W.

southeast China. Entry of Al into titanite usually also involves entry of Nb, through the double substitutions $Na^{+} + Nb^{5+} \leftrightarrow Ca^{2+} + Ti^{4+}$ and $(Al, Fe)^{3+} + Nb^{5+} \leftrightarrow 2Ti^{4+}$ (Černý *et al*., 1995; Liferovich and Mitchell, 2005). Where the entry of Al^{3+} is not matched by the entry of a univalent element such as Na, the substitution scheme may well be $(Al + Fe)^{3+} + (F,OH)^{-} \rightarrow Ti^{4+} + O^{2-}$ (Perseil and Smith, 1995; Della Ventura *et al*., 1999; Liferovich and Mitchell, 2005). Such a scheme is consistent with the significant F contents in the Keivy sample (1.65–2.20 wt.%; 0.174–0.231 a.p.f.u.). We note, however, that the F contents are unusually high; Pan *et al*. (1993), for example, recorded levels of 0.00–0.46 wt.% in unaltered and altered titanite from a range of igneous rocks. Alternatively, the F may have been incorporated into a submicroscopic phase, such as fluocerite or *REE*-carbonate, not detected by us. Water contents, calculated from the charge balance, are 0.8–0.9 wt.%, raising analytical totals to ~98 wt.%.

Conversely, the total *REE* content is low, being much lower than that often found in peralkaline and alkaline parageneses (≤0.55 a.p.f.u., Della Ventura *et al*., 1999; Chakmouradian and Mitchell, 1999). Liferovich and Mitchell (2005), however, also recorded low *REE* contents (≤0.012 a.p.f.u.) in their Khibiny samples. In 160b/62, it is the *LREE* which are low; Y levels are relatively high (average 0.030 a.p.f.u.; 3.45 wt.% Y_2O_3).

Aeschynite-(Y) and aeschynite-(Ce)

The (*REE*, U, Th)-(Ti, Nb, Ta) oxide phase has been classified as a member of the aeschynite group on the basis of the three-group canonical discriminant of Ercit (2005) (Fig. 8). Members of the group have the general formula AB_2O_6, where A represents *REE*, Ca, U and Th and B represents Ti, Nb and Ta. Electron microprobe analyses of aeschynite are presented in Table 5 and Supplementary Table 2*b* (deposited at www.minersoc.org/pages/e_journals/dep_mat_mm.html). Formulae were calculated on the basis of two cations in the *B* site and with all Fe as Fe^{2+}. Cation site allocations are shown in Table 5. The oxide totals are relatively high (95.67–98.38 wt.%), the lower values possibly representing the presence of water and unanalysed oxides; e.g. Aurisicchio *et al*. (2001) found both hydroxyl and molecular water, using infrared spectra, in aeschynite-(Y) from pegmatites in the

https://doi.org/10.1180/minmag.2015.079.5.02 Published online by Cambridge University Press

Baveno pink granite, Italy. The cation sums range from 2.91 to 3.07 a.p.f.u. (average 2.99), close to the ideal value of 3.0. The occupancy of the *A* site is slightly variable, e.g. Ce 0.072–0.282 a.p.f.u. and Y 0.138–0.363 a.p.f.u. The majority of analyses are aeschynite-(Y) but in six analytical points, Ce exceeds Y. There is a relatively high Nd content (0.090–0.185 a.p.f.u.), indicating significant substitution towards aeschynite-(Nd). Thorium abundances are high and variable (2.86–15.61 wt.% ThO_2; 0.040–0.217 a.p.f.u.) whilst U is low (0.21–1.41 wt.% UO_2; 0.003–0.019 a.p.f.u.). In the *B* site, Ti ranges from 1.112–1.419 a.p.f.u. and Nb from 0.414–0.833 a.p.f.u. Tantalum levels are low (≤0.021 a.p.f.u.) and Nb/Ta ratios correspondingly high (37–91). The Fe content is low (0.39–4.21 wt.% FeO* (total Fe as Fe^{2+}); 0.020–0.209 a.p.f.u.) and there are trace amounts of W (≤0.008 a.p.f.u.).

Compositional variation can generally be represented by two end-members, one higher in Ti, Th, U and Fe, the other higher in Nb and *LREE*. These differences are partly reflected in the core and rim compositions of the largest crystal analysed by us, with the addition that the *HREE* are slightly higher in the rim (Table 5). Aeschynite compositions in the chevkinite-(Ce) zone are broadly similar to those in the (ferri)allanite-(Ce) zone, as implied by the overlap in Fig. 8. There are, however, some differences; for example, the average Ce/Y ratio in the chevkinite-(Ce) zone is 0.87, in the allanite-(Ce) zone 0.47. On the basis of currently available data, there appears to be no relationship between composition and location within the (ferri)allanite-(Ce) zone.

Chondrite-normalized *REE* patterns are shown in Fig. 9; generally, there is enrichment from La to Nd and then a decrease through the *HREE*, with negative Eu anomalies (Eu/Eu* 0.31–1.00). Broadly similar patterns have been described in aeschynite-(Ce) from a vein in the contact aureole of the Adamello batholith, Italy, by Gieré and Williams (1992) and in aeschynite-(Ce), aeschynite-(Y) and aeschynite-(Nd) from pegmatites of the Třebič Pluton, Czech Republic, by Škoda and Novák (2007). The aeschynite compositions are shown in terms of *A*- and *B*-site occupancy in Fig. 10, along with data for various comparative suites. Aeschynites from Keivy 160b/62, the Baveno pink granite, El Muerto pegmatite and Pyrenean albitites are distributed along trends suggesting major control by substitution 2, *viz*. $(U,Th)^{4+} + Ti^{4+} = (Y,REE)^{3+} + (Nb,Ta)^{5+}$. Each of the El Muerto and Baveno suites contains an anomalously Ca-rich analysis; these are connected to the main field by arrows in Fig. 10 and may represent a separate control by substitution 5, $(2Ca^{2+} + 3(Nb,Ta)^{5+} = (U,Th)^{4+} + (Y,REE)^{3+} + 3Ti^{4+})$. Although showing limited compositional variation, aeschynite-(Y) from the Wentworth pluton, Nova Scotia, parallels substitution 1, $Ca^{2+} + (Nb,Ta)^{5+} = (Y,REE)^{3+} + Ti^{4+}$. Pegmatites of the Třebič Pluton, Czech Republic, host an unusually wide range of aeschynite phases, *viz*. aeschynite-(Y), aeschynite-(Ce), aeschynite-(Nd), nioboaeschynite-(Ce) and 'tantalaeschynite-(Ce)' (Škoda and Novák, 2007). The compositional variation may be related to a combination of substitutions 1 and 5 (Škoda and Novák, 2007).

REE-carbonates

Analysis of the *REE*-carbonates has been limited by the small size of the majority of grains; six EMP analyses are given in Supplementary Table 2*c* (available from www.minersoc.org/pages/e_journals/dep_mat_mm.html), with formulae calculated on the basis of one cation. The compositions in the chevkinite and allanite zones are rather different. Those in the chevkinite zone are bastnäsite-(Ce) and hydroxylbastnäsite-(Ce) showing low Ca (≤0.205 a.p.f.u.) and Fe (≤0.004 a.p.f.u.), and, in the bastnäsite-(Ce), F contents (0.91–0.93 a.p.f.u.) close to the theoretical maximum. The allanite zone also contains hydroxylbastnäsite-(Ce), but a grain close to the primary zircon crystal (Fig. 4*d*) is apparently an extremely fine intergrowth of hydroxylbastnäsite-(Ce) and hydroxylparisite-(Ce) (Ca 0.152–0.205 a.p.f.u.).

Discussion

Inferred sequence of events

From the textural relationships and mineral compositions, the following sequence of events may be inferred.

Stage 1a. The formation of the altered chevkinite zone was described in Bagiński *et al*. (2015) (Figs 3*a*, 4*a*). Chevkinite-(Ce) was hydrothermally altered, initially with removal of *REE*, Fe and Si, enrichment in Ca and slight enrichment in Ti. Some *REE* were tied up in aeschynite-(Ce), aeschynite-(Y) and bastnäsite-(Ce) and some Fe in aeschynite-(Y). This was followed by further removal of *REE*, Si and Ca, strong Ti enrichment and more modest Nb and Th enrichment.

https://doi.org/10.1180/minmag.2015.079.5.02 Published online by Cambridge University Press

TABLE 5. Representative EMP analytical results for aeschynite in 160b/62.

	in unaltered chevkinite zone					in ferri(allanite) zone				
Anal. No.	1	2	3	4	5	6	7	8	9	10
wt.%										
WO_3					0.35	0.82	0.78	0.38	0.64	0.56
P_2O_5	b.d.	0.05	b.d.	b.d.	b.d.	b.d.	b.d.	b.d.	0.08	0.03
Nb_2O_5	25.64	25.48	30.05	17.29	27.87	20.34	14.97	24.18	20.75	18.10
Ta_2O_5	0.47	0.90	0.96	0.58	1.26	0.39	0.36	1.02	0.46	0.34
TiO_2	27.02	26.08	24.54	30.36	25.11	29.14	30.84	26.94	29.37	30.32
ThO_2	9.32	4.04	2.86	9.31	2.92	7.18	15.61	4.79	9.15	10.42
UO_2	0.53	0.88	0.66	0.31	0.27	0.55	1.05	0.52	0.59	1.41
Y_2O_3	7.53	5.88	4.24	7.46	7.60	5.82	9.04	9.78	7.67	11.24
La_2O_3	1.46	2.92	3.30	0.75	2.18	2.00	0.65	1.21	1.49	0.75
Ce_2O_3	7.06	10.43	12.57	4.98	9.42	8.99	3.21	6.16	7.06	3.56
Pr_2O_3	0.99	1.58	1.73	1.04	1.65	1.28	0.60	1.26	1.34	0.49
Nd_2O_3	4.84	6.80	7.08	6.03	8.09	8.56	4.14	7.23	6.19	4.53
Sm_2O_3	1.90	2.25	1.86	3.43	2.32	2.24	1.87	2.52	1.42	1.63
Eu_2O_3	b.d.	0.60	b.d.	0.30	0.50	0.20	b.d.	0.66	0.27	0.51
Gd_2O_3	2.89	2.21	2.00	3.60	3.06	2.90	2.65	2.98	2.44	2.62
Tb_2O_3	0.38	0.28	0.33	0.36	0.23	0.22	0.23	0.20	0.39	0.30
Dy_2O_3	2.02	0.94	1.18	2.06	1.41	1.22	1.96	1.73	1.85	2.07
Er_2O_3					0.70	0.61	1.17	1.02	0.85	1.43
Yb_2O_3	0.42	0.28	b.d.	0.27	0.60	0.34	0.85	0.63	0.41	0.82
CaO	1.02	1.12	1.59	1.81	1.54	1.25	2.42	1.75	1.07	1.86
MnO	b.d.	b.d.	b.d.	b.d.	b.d.	0.12	b.d.	b.d.	0.10	0.15
FeO*	0.55	0.94	0.39	1.84	1.05	2.10	3.03	2.79	1.65	2.17
PbO	1.02	0.69	0.56	0.83		0.43	0.31		b.d.	0.63
Total	95.06	94.35	95.90	92.61	98.13	96.70	95.74	97.75	95.24	95.94
CV1	6.28	7.10	6.96	6.55	7.41	7.67	5.97	6.93	6.80	6.64
CV2	0.65	0.96	1.02	0.26	2.21	1.40	0.78	2.35	1.03	1.54

(continued)

Table 5 (*contd.*)

Formulae on the basis of *B* cations = 2										
Ca	0.067	0.075	0.104	0.120	0.101	0.081	0.159	0.111	0.069	0.121
La	0.033	0.067	0.075	0.017	0.049	0.045	0.015	0.026	0.033	0.017
Ce	0.159	0.237	0.282	0.113	0.211	0.199	0.072	0.133	0.156	0.079
Pr	0.022	0.036	0.039	0.023	0.037	0.028	0.013	0.027	0.030	0.011
Nd	0.106	0.151	0.155	0.133	0.177	0.185	0.090	0.158	0.134	0.098
Sm	0.040	0.048	0.039	0.073	0.049	0.047	0.039	0.051	0.030	0.034
Eu	0.000	0.013	0.000	0.006	0.010	0.004	0.000	0.013	0.000	0.011
Gd	0.059	0.046	0.041	0.074	0.062	0.058	0.054	0.058	0.049	0.053
Tb	0.008	0.006	0.007	0.007	0.005	0.004	0.005	0.004	0.008	0.006
Dy	0.040	0.019	0.023	0.041	0.028	0.024	0.039	0.033	0.036	0.040
Er					0.013	0.012	0.022	0.019	0.016	0.027
Yb	0.008	0.005	0.000	0.005	0.011	0.006	0.016	0.011	0.008	0.015
Y	0.247	0.195	0.138	0.245	0.247	0.187	0.294	0.307	0.247	0.363
Mn	0.000	0.000	0.000	0.000	0.000	0.006	0.000	0.000	0.005	0.008
Th	0.131	0.057	0.040	0.131	0.041	0.099	0.217	0.064	0.126	0.144
U	0.007	0.012	0.009	0.004	0.004	0.007	0.014	0.007	0.008	0.019
Pb	0.017	0.012	0.009	0.014		0.007	0.005		0.002	0.010
P	0.000	0.000	0.000	0.000	0.000	0.000	0.000	0.000	0.004	0.000
Sum *A*	0.944	0.979	0.961	1.006	1.046	1.000	1.054	1.022	0.961	1.056
Ti	1.250	1.220	1.131	1.412	1.155	1.324	1.418	1.197	1.336	1.383
Nb	0.713	0.716	0.833	0.483	0.771	0.556	0.414	0.646	0.567	0.496
Ta	0.008	0.015	0.016	0.010	0.021	0.006	0.006	0.016	0.008	0.006
Fe^{2+}	0.028	0.049	0.020	0.095	0.054	0.106	0.155	0.138	0.083	0.110
W					0.003	0.007	0.007	0.003	0.006	0.005
Σ cations	2.94	2.98	2.96	3.01	3.05	3.00	3.05	3.02	2.96	3.06

FeO*, all Fe as Fe2+. b.d., below detection. Blank, not determined. CV1, CV2, canonical variables of Ercit (2005).
Analyses 9 and 10 are of the core and rim of the large (35 μm) crystal mentioned in the text.

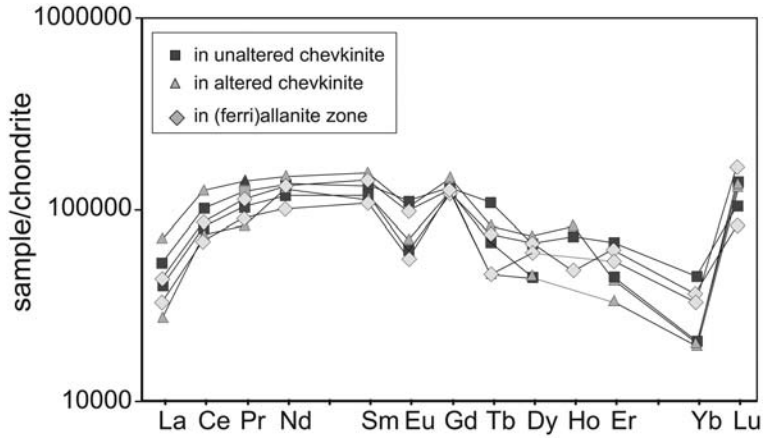

FIG. 9. Chondrite-normalized *REE* patterns for aeschynite. Normalizing factors from Sun and McDonough (1989). Samples used: Supplementary Table 2*b*, numbers 1, 3, 28, 29, 30, 35.

Stage 1b. Essentially at the same time as stage 1a, there was formation of ferriallanite-(Ce), davidite-(La), aeschynite-(Ce) and *REE*-carbonates, the ferriallanite-(Ce) rimming the altered chevkinite and penetrating into it as fingers and patches (Figs 3, 4*a*). The additional Al^{3+} and Ca^{2+} involved in the reaction were probably supplied to the fluid during the metasomatic alteration of the host body.

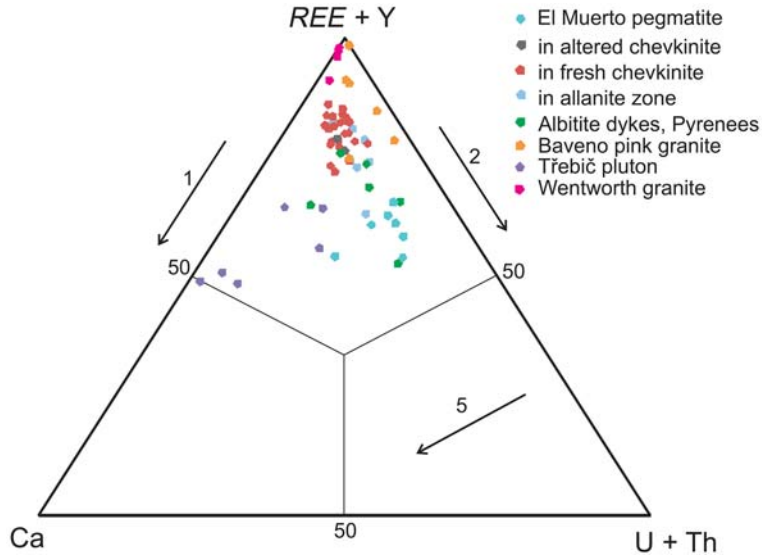

FIG. 10. Chemical composition of aeschynite-(Y) from Keivy sample 160b/62 plotted in terms of *A*-site occupancy, along with data for comparative suites. Data from Supplementary Table 2b. The numbered arrows represent substitutions, as explained in the text (Škoda and Novák, 2007). Other data sources: pegmatites in the Baveno pink granite (Aurisicchio *et al*., 2001), albitite dykes, Pyrénées, France (Monchoux *et al*., 2006), El Muerto pegmatite, Oaxaca, Mexico (Prol-Ledesma *et al*., 2012), pegmatites in the Třebič Pluton, Czech Republic (Škoda and Novák, 2007) and the Wentworth Pluton, Nova Scotia (Papoutsa and Pe-Piper, 2013). The fields of Baveno and El Muerto analytical results have been drawn to exclude one anomalously Ca-rich data point in each case. The dashed arrows indicate a possible control by substitution 5.

https://doi.org/10.1180/minmag.2015.079.5.02 Published online by Cambridge University Press

Stage 2. Further away from the unaltered chevkinite-(Ce), there was replacement of ferriallanite-(Ce) by allanite-(Ce) and of davidite-(La) by rutile, with subsequent replacement of rutile by titanite and quartz (Figs 4*b*,*c*,*d*). There was continued crystallization of aeschynite-(Y) and *REE*-carbonates.

Stage 3. Finally, the rutile-titanite pods were partially altered to chlorite.

Nature of the hydrothermal fluids

The mineral assemblage of the host metasomatite includes feldspar, epidote and Ca-Na-amphibole, attesting to the alkaline nature of the hydrothermal fluids. The replacement of chevkinite-(Ce) by ferriallanite-(Ce) and then by allanite-(Ce) and the replacement of rutile by titanite and quartz indicate that, in particular, the fluids had high Ca and Si activities (Lumpkin *et al*., 2013). The occurrence of F in bastnäsite-(Ce) and titanite points to a significant F component in the fluid. The increased Ca content and lower F content in *REE*-carbonate furthest from the unaltered chevkinite-(Ce) may suggest that the F content of the fluid became lower as alteration proceeded.

The presence of *REE*-carbonates at all stages of alteration indicates that the fluids were CO_2-bearing. Furthermore, Rolland *et al*. (2003) suggested that hydrothermal fluids with high XCO_2 (0.2–0.8) are associated with bastnäsite with high La/Nd ratios (~4–5), whereas bastnäsite formed from fluids with very low CO_2 contents has low La/Nd (0.6–2). On that basis, the La/Nd ratios of the bastnäsite in 160b/62 (1.5–3.9) would indicate a significant CO_2 component in the fluids.

Rutile – titanite – aeschynite relationships

The stability relationships between the Ti-bearing phases in alkaline parageneses are complex. Pan *et al*. (1993) described late hydrothermal alteration of titanite with the formation of *REE*-minerals in the crystals or along crystal boundaries, concluding that the *REE*-minerals were formed from *REE* leached from the titanite. Allen *et al*. (1986) reported secondary *REE*-minerals along fractures and grain boundaries in titanite from the Closepet Batholith, south India. Della Ventura *et al*. (1999) reported a *REE*,Th,U,Ca-silicate, possibly britholite, in a suite of mineral inclusions in altered titanite from Tre Croci, Vico complex, Italy, but suggested that at least some of the *REE* present in the rock were supplied by an external source. Wang *et al*. (2001) argued that titanite is stable under relatively low f_{CO_2} conditions, being replaced at higher f_{CO_2} by rutile and a carbonate mineral. Papoutsa and Pe-Piper (2013) suggested that an undetermined TiO_2 mineral in the Wentworth Pluton, Nova Scotia, was formed from titanite during hydrothermal alteration. Lumpkin *et al*. (2013) presented reactions illustrating the breakdown of davidite to titanite and rutile, the relative proportions of the products reflecting the availability of Si and Ca.

The textural evidence seems clear that rutile in 160b/62, formed by breakdown of davidite-(La), was itself replaced by titanite and quartz as alteration progressed. The compositional differences suggest that Ca, Si and *REE* were supplied by the hydrothermal fluids.

Information on the relationships between aeschynite and other Ti-bearing phases is rather scarce. Uher *et al*. (2009) reported Nb-rich rutile (?) intergrown with aeschynite/polycrase-(Y), ~20 μm in size, in metamorphosed A-type granites of the Turčok massif, Slovakia. Papoutsa and Pe-Piper (2013) found, in the Wentworth granite, that aeschynite-(Y) occurs only in close proximity to, and post-dated, titanite. They suggested that breakdown of titanite to a TiO_2 phase released Ca and Si but left residual Ti. The Ti reacted with earlier-formed *REE*-bearing fluids to produce aeschynite-(Y). Prol-Ledesma *et al*. (2012) reported, from albitized zones of the El Muerto pegmatite, Mexico, titanite being replaced along grain borders by a fine-grained association of niobian rutile, thorutite, polycrase-(Y), uranopolycrase and aeschynite-(Y). In 160b/62, aeschynite-(Y) and aeschynite-(Ce) occur in the unaltered and altered chevkinite zones and in the allanite zone, sometimes but not invariably associated with, and derived from, titanite or rutile. Whilst it is difficult to determine on textural grounds if the aeschynite in the altered chevkinite and allanite zones represents a new phase or modification of primary crystals, we have assumed above that they were largely secondary, incorporating Nb, Ti, *REE*, Y and Th released from the major phases during alteration.

Acknowledgements

The authors are grateful to Ms Lidia Jeżak for help with microprobe analyses. Financial support was provided by Nardowe Centrum Nauki (National Science Centre) grant number N N307 634040. Igor Broska and two anonymous referees are thanked for helpful reviews of the original manuscript.

https://doi.org/10.1180/minmag.2015.079.5.02 Published online by Cambridge University Press

References

Allen, P., Condie, K.C. and Bowling, G.P. (1986) Geochemical characteristics and possible origins of the Closepet Batholith, south India. *Journal of Geology*, **94**, 283–299.

Aurisicchio, C., De Vito, C., Ferrini, V. and Orlandi, P. (2001) Nb-Ta oxide minerals from miarolitic pegmatites of the Baveno pink granite, NW Italy. *Mineralogical Magazine*, **65**, 509–522.

Back, M.E. and Mandarino, J.A. (2008) *Fleischer's Glossary of Mineral Species 2008*. The Mineralogical Record Inc., Tucson, USA.

Bagiński, B., Macdonald, R., Dzierżanowski, P., Zozulya, D. and Kartashov, P.M. (2015) Hydrothermal alteration of chevkinite-group minerals: products and mechanisms. Part 1. Hydration of chevkinite-(Ce). *Mineralogical Magazine*, **79**, 1019–1037.

Belkin, H.E., Macdonald, R. and Grew, E.S. (2009) Chevkinite-group minerals from granulite-facies metamorphic rocks and associated pegmatites of East Antarctica and South India. *Mineralogical Magazine*, **73**, 149–164.

Carlier, G and Lorand, J.-P. (2008) Zr-rich accessory minerals (titanite, perrierite, zirconolite, baddeleyite) record strong oxidation associated with magma mixing in the south Peruvian potassic province. *Lithos*, **104**, 54–70.

Černý, P., Novak, M. and Chapman, R. (1995) The Al(Nb, Ta)Ti_2 substitution in titanite: the emergence of a new species. *Mineralogy and Petrology*, **52**, 61–73.

Chakmouradian, A.R. and Mitchell, R.H. (1999) Primary, agpaitic and deuteric stages in the evolution of accessory Sr, REE, Ba and Nb-mineralization in nepheline-syenite pegmatites at Pegmatite Peak, Bearpaw Mts, Montana. *Mineralogy and Petrology*, **67**, 85–110.

Della Ventura, G., Bellatreccia, F. and Williams, C.T. (1999) Zr- and LREE-rich titanite from Tre Croci, Vico volcanic complex (Latium, Italy). *Mineralogical Magazine*, **63**, 123–130.

Ercit, T.S. (2005) Identification and alteration trends of granitic-pegmatite-hosted (Y,REE,U,Th)-(Nb,Ta,Ti) oxide minerals: a statistical approach. *The Canadian Mineralogist*, **43**, 1291–1303.

Gatehouse, B.M., Grey, I.E. and Kelly, P.R. (1979) The crystal structure of davidite. *American Mineralogist*, **64**, 1010–1017.

Gieré, R. and Williams, C.T. (1992) REE-bearing minerals in a Ti-rich vein from the Adamello contact aureole (Italy). *Contributions to Mineralogy and Petrology*, **112**, 83–100.

Green, T.H. and Pearson, N.J. (1987) High-pressure, synthetic loveringite-davidite and its rare earth element geochemistry. *Mineralogical Magazine*, **51**, 145–149.

Haggerty, S.E., Smyth, J.R., Erlank, A.J., Rickard, R.S. and Danchin, R.V. (1983) Lindsleyite (Ba) and mathiasite (K): two new chromium-titanates in the crichtonite series from the upper mantle. *American Mineralogist*, **68**, 495–505.

Harlov, D.E., Wirth, R. and Hetherington, C.J. (2011) Fluid-mediated partial alteration in monazite: the role of coupled dissolution-reprecipitation in element redistribution and mass transfer. *Contributions to Mineralogy and Petrology*, **162**, 329–348.

Hirtopanu, P., Andersen, J.C., Fairhurst, R.J. and Jakab, G. (2013) Allanite-(Ce) and its associations, from the Ditrau intrusive massif, East Carpathians, Romania. *Proceedings of the Romanian Academy, Series B*, **2013**, 59–74.

Jiang, N. (2006) Hydrothermal alteration of chevkinite-(Ce) in the Shuiquangou syenitic intrusion, northern China. *Chemical Geology*, **227**, 100–112.

Liferovich, R.P. and Mitchell, R.H. (2005) Composition and paragenesis of Na-, Nb- and Zr- bearing titanite from Khibina, Russia, and crystal-structure data for synthetic analogues. *The Canadian Mineralogist*, **43**, 795–812.

Lumpkin, G.R., Blackford, M.G. and Colella, M. (2013) Chemistry and radiation effects of davidite. *American Mineralogist*, **98**, 275–278.

Macdonald, R. and Belkin, H.E. (2002) Compositional variation in minerals of the chevkinite group. *Mineralogical Magazine*, **66**, 1075–1098.

Macdonald, R., Belkin, H.E., Wall, F. and Bagiński, B. (2009) Compositional variation in the chevkinite group: new data from igneous and metamorphic rocks. *Mineralogical Magazine*, **73**, 777–796.

Macdonald, R., Bagiński, B., Kartashov, P., Zozulya, D. and Dzierżanowski, P. (2012) Chevkinite-group minerals from Russia and Mongolia: new compositional data from metasomatites and ore deposits. *Mineralogical Magazine*, **76**, 535–549.

Macdonald, R., Bagiński, B., Dzierżanowski, P., Fettes, D.J. and Upton, B.G.J. (2013) Chevkinite-group minerals in UK Palaeogene granites: underestimated REE-bearing accessory phases. *The Canadian Mineralogist*, **51**, 333–347.

Monchoux, P., Fontan, F., De Parseval, P., Martin, R.F. and Wang, R.C. (2006) Igneous albitite dikes in orogenic lherzolites, Western Pyrénées, France: a possible source for corundum and alkali feldspar xenocrysts in basaltic terrnaes. 1. Mineralogical associations. *The Canadian Mineralogist*, **44**, 817–842.

Olerud, S. (1988) Davidite-loveringite in early Proterozoic albite felsite in Finnmark, north Norway. *Mineralogical Magazine*, **52**, 400–402.

Pan, Y., Fleet, M.E., MacRae, N.D. (1993) Late alteration in titanite ($CaTiSiO_5$): redistribution and remobilization of rare earth elements and implications for U/Pb and Th/Pb geochronology and nuclear waste

https://doi.org/10.1180/minmag.2015.079.5.02 Published online by Cambridge University Press

disposal. *Geochimica et Cosmochimica Acta*, **57**, 355–367.

Papoutsa, A.D. and Pe-Piper, G. (2013) The relationship between REE-Y-Nb-Th minerals and the evolution of an A-type granite, Wentworth Pluton, Nova Scotia. *American Mineralogist*, **98**, 444–462.

Perseil, E.-A. and Smith, D.C. (1995) Sb-rich titanite in the manganese concentrations at St. Marcel-Praborna, Aosta Valley, Italy: petrography and crystal-chemistry. *Mineralogical Magazine*, **59**, 717–734.

Petrik, I., Broska, I., Lipka, J. and Siman, P. (1995) Granitoid allanite-(Ce) substitution relations, redox conditions and REE distributions (on an example of I-type granitoids, Western Carpathians, Slovakia). *Geologica Carpathica*, **46**, 79–94.

Prol-Ledesma, R.-M., Melgarejo, J.C. and Martin, R.F. (2012) The El Muerto "NYF" granitic pegmatite, Oaxaca, Mexico, and its striking enrichment in allanite-(Ce) and monazite-(Ce). *The Canadian Mineralogist*, **50**, 1055–1076.

René, M. and Škoda, R. (2011) Nb-Ta-Ti oxides fractionation in rare-metal granites: Krásno-Horni Slavkov ore district, Czech Republic. *Mineralogy and Petrology*, **103**, 37–48.

Rolland, Y., Cox, S., Boullier, A.-M., Pennacchioni, G. and Mancktelow, N. (2003) Rare earth and trace element mobility in mid-crustal shear zones: insights from the Mont Blanc Massif (Western Alps). *Earth and Planetary Science Letters*, **214**, 203–219.

Savel'eva, V.B. and Karmanov, N.S. (2008) REE minerals of alkaline metasomatic rocks in the Main Sayan Fault. *Geology of Ore Deposits*, **50**, 681–696.

Škoda, R. and Novák, M. (2007) Y,REE,Nb,Ta,Ti-oxide (AB_2O_6) minerals from REL-REE euxenite-subtype pegmatites of the Třebič Pluton, Czech Republic; substitutions and fractionation trends. *Lithos*, **95**, 43–57.

Sun, S.-S. and McDonough, W.F. (1989) Chemical and isotopic systematics of oceanic basalts: applications for mantle composition and processes. Pp. 313–345 in: *Magmatism in the Ocean Basins* (A.D. Saunders and M.J. Norry, editors.). Special Publication of the Geological Society, **42**. Geological Society, London.

Uher, P., Ondrejka, M. and Konečny, P. (2009) Magmatic and post-magmatic Y-REE-Th phosphate, silicate and Nb-Ta-Y-REE oxide minerals in A-type metagranite: an example from the Turčok massif, the Western Carpathians, Slovakia. *Mineralogical Magazine*, **73**, 1009–1025.

Vlach, S.R.F. and Gualda, G.A.R. (2007) Allanite and chevkinite in A-type granites and syenites of the Graciosa Province, southern Brazil. *Lithos*, **97**, 98–121.

Wang, R.-C., Wang, D.-Z., Zhao, G.-T., Lu, J.-J., Chen, X.-M. and Xu, S.-J. (2001) Accessory mineral record of magma-fluid interaction in the Laoshan I- and A-type granitic complex, Eastern China. *Physics and Chemistry of the Earth (A)*, **26**, 835–849.

Wood, S.A. and Williams-Jones, A.E. (1994) The aqueous geochemistry of the rare-earths and yttrium. 4. Monazite solubility and REE mobility in exhalative massive-sulfide depositing environments. *Chemical Geology*, **115**, 47–60.

Xie, L., Wang, R.C., Wang, D.Z. and Qu, J.S. (2006) A survey of accessory mineral assemblages in peralkaline and more aluminous A-type granites of the southeast coastal area of China. *Mineralogical Magazine*, **70**, 709–729.

Zozulya, D.R. and Eby, G.N. (2010) Rare-metal ore occurrences, related to the Late Archean A-type granites from the Keivy zone (NE Fennoscandian shield). Pp. 113–115 in: *International conference on A-type granites and related rocks through time, Abstract Volume* (O.T. Ramo, S.R. Lukari and A.P. Heinonen, editors). IGCP 510, Helsinki.

Zozulya, D.R., Eby, G.N. and Bayanova, T.B. (2001) Keivy alkaline magmatism in the NE Baltic Shield: evidence for the presence of an enriched reservoir in Late Archaean mantle. Pp. 540–542 in: *4th International Archaean Symposium 2001. Extended Abstracts, Record 2001/37.* (K.F. Cassidy, J.M. Dunphy and M.J. Kranendank, editors). AGSO-Geoscience Australia, Perth, Western Australia.

Zozulya, D.R., Bayanova, T.B. and Eby, G.N. (2005) Geology and age of the Late Archean Keivy alkaline province, northeastern Baltic Shield. *Journal of Geology*, **113**, 601–608.

https://doi.org/10.1180/minmag.2015.079.5.02 Published online by Cambridge University Press